PCCP

PAPER

Cite this: *Phys. Chem. Chem. Phys.*, 2019, **21**, 13835

Inducing magnetism in non-magnetic α-$FeSi_2$ by distortions and/or intercalations†

Vyacheslav Zhandun, *[a] Natalia Zamkova,[a] Pavel Korzhavyi[b] and Igor Sandalov[a]

Received 26th April 2019,
Accepted 3rd June 2019

DOI: 10.1039/c9cp02361e

rsc.li/pccp

By means of hybrid *ab initio* + model approach we show that the lattice distortions in non-magnetic α-$FeSi_2$ can induce a magnetic state. However, we find that the distortions required for the appearance of magnetism in non-magnetic α-$FeSi_2$ are too large to be achieved by experimental fabrication of thin films. For this reason we suggest a novel way to introduce magnetism in α-$FeSi_2$ using "chemical pressure" that is, intercalating the α-$FeSi_2$ films by light elements. Theoretical study of the distortions resulting from intercalation reveals that the most efficient intercalants for formation of magnetism and a high spin polarization are lithium, phosphorus and oxygen. Investigation of the dependency of the magnetic moments and spin polarisation on the intercalation atoms concentration shows that the spin polarization remains high even at small concentrations of intercalated atoms, which is extremely important for modern silicate technology.

I. Introduction

The modern semiconductor industry is mainly based on silicon.[1] The development of spintronics demands new magnetic materials that are compatible with silicon. These facts motivate a search for transition metal silicides which are either magnetic or close to magnetic instability. The ability of iron to form a vast variety of magnetic compounds with silicon, both in the bulk and in the epitaxially stabilized forms, makes it especially attractive. These compounds are already used in micro- and optoelectronics, and also in photovoltaics.[2–6] Iron disilicide, α-$FeSi_2$, is unstable and non-magnetic in the bulk form. For these reasons it was not in the front line of the list of candidates for application. The situation changed after publications[7–9] in which it was shown that the film and nanoparticles of α-$FeSi_2$ can be stabilized epitaxially. Moreover, this causes it to become magnetic. The nature of this phenomenon is not understood.

We assume that certain lattice distortions can cause magnetism. The experimental data for films[7] and nanoparticles[8,9] of α-$FeSi_2$, as well as the theoretical analysis,[10] support this point of view. Why this may favor magnetic moment formation can be seen from the second-order admixture of neighboring-atom (nAt) states with the d-electron bands. Indeed, an itinerant magnetism arises due to peaks in the densities of electron state. These peaks originate either from the presence of narrow bands, or from flat areas on the Fermi surface. If a band has a large bandwidth and does not contain sufficiently narrow DOS peaks in the vicinity of the Fermi energy, a Stoner-like criterion for magnetism is not fulfilled and a magnetic moment (MM) is not formed. Therefore, any mechanism which favors a decrease of width in the effective d-band will also favor the formation of magnetism. An increase of the distance between an Fe atom and nAt decreases the hopping matrix element $t_{Fe-nAt}(k)$ and, therefore, the effective width of the d-band decreases too, thus making the fulfilment of the Stoner's criterion easier.

Earlier discussions were focused on the effect of the in-plane distortions caused by the misfit strains.[10] Recent experimental data[11] suggest that out-of-plane distortions in α-$FeSi_2$ nanoparticles also arise. The observed magnetic moments are quite small[7,11] $\sim 0.2\ \mu_B$. Theoretical analysis of the formation of magnetism in iron silicides[10] shows that the small lattice distortions which arise during film fabrication may cause small moments. It is reasonable to assume that a further increase of these distortions may increase the magnetic moments. In all these experiments the distortions arise due to and in the vicinity of the interface. It is highly desirable to create distortions which are not linked to the interface, but are caused by other reasons. We suggest to exploit the fact that the crystal structure of iron disilicide, α-$FeSi_2$, has a cavity formed by the Si planes. Sufficiently small atoms can be intercalated into this cavity and cause distortions which, in turn, induce magnetism.

In the present work we investigate such a possibility by inspecting the intercalation of α-$FeSi_2$ with different light elements. We use an *ab initio* (VASP, DFT-GGA, see 2) approach along with a hybrid *ab initio* and a model developed in ref. 10 and 12.

[a] *Kirensky Institute of Physics, Federal Research Center "Krasnoyarsk Science Centre, Siberian Branch of the Russian Academy of Sciences", 660036 Krasnoyarsk, Russia. E-mail: jvc@iph.krasn.ru*

[b] *Kungliga Tekniska Högskolan, SE-100 44 Stockholm, Sweden*

† Electronic supplementary information (ESI) available. See DOI: 10.1039/c9cp02361e

The results of DFT-GGA calculations are mapped onto the multiorbital model suggested in ref. 12. The mapping is based on the idea to exploit the Hohenberg–Kohn theorem, equalizing the charge densities generated by the Kohn–Sham equations and obtained from the Hartree–Fock equations for the model Hamiltonian. Due to the success of the Kohn–Sham approach in description of real materials, we treat the corresponding charge density as a "genuine" one and find the parameters of the model Hamiltonian from the minimization of difference between the Kohn–Sham and the model Hartree–Fock charge densities.

The consideration of the model allows us (i) to find out if the critical line separating magnetic from non-magnetic states exists on its phase diagram or not; and (ii) if yes, to reveal which of the model parameters controls the point of the real-material position with respect to this critical line. Further this knowledge is used for the *ab initio* modeling of the situation where the critical parameter is changed into the desired direction.

The paper organised as follows. In Section II, we provide the details of the *ab initio* and the model calculations. The effect of the lattice distortions in α-$FeSi_2$ on the magnetic moment formation in both approaches is described in Section IIIA. Section IIIB presents the results of the calculations for a-$FeSi_2$ with intercalated atoms. Section IV contains the conclusions.

II. Calculation details

A. *Ab initio* part

All *ab initio* calculations presented here have been performed using the Vienna *ab initio* simulation package (VASP)[13] with projector augmented wave (PAW) pseudopotentials.[14] The valence electron configuration $3d^64s^2$ is taken for the Fe atoms, and $3s^23p^2$ is taken for the Si atoms. The calculations are based on density functional theory (DFT) in the generalized gradient approximation (GGA), where the exchange–correlation functional is chosen within the Perdew–Burke–Ernzerhof (PBE) parametrization.[15] Throughout all calculations, the plane-wave cutoff energy was 500 eV, and the Gauss broadening with a smearing of 0.05 eV was used. The Brillouin-zone integration was performed on a $15 \times 15 \times 8$ Monkhorst–Pack grid[16] of special points. The optimized lattice parameters and atomic coordinates were obtained by minimizing the total energy.

B. Model part

In ref. 12 we suggested to combine the *ab initio* and model calculations by means of the following scheme. First, we perform *ab initio* calculations of electronic and magnetic properties within the framework of DFT-GGA. Then we map the DFT-GGA results onto the multiorbital model suggested in ref. 12. The details of model calculations are described in ref. 12. Here we give only the Hamiltonian and the general parameters of the model. We use the set of the Kanamori interactions[17] between the d-electrons of Fe (five d-orbitals per spin). The crystal structure contains neighboring Fe ions; for this reason the direct interatomic d–d-exchange and d–d-hopping have to be included. The Si p-electrons (three p-orbitals per spin) are modeled by atomic levels and interatomic hopping. Both subsystems are connected *via* d–p-hopping. Thus, the Hamiltonian of the model is:

$$H = H^{\mathrm{Fe}} + H_{J'}^{\mathrm{Fe-Fe}} + H_0^{\mathrm{Si}} + H_{\mathrm{hop}}, \tag{1}$$

where

$$H^{\mathrm{Fe}} = H_0^{\mathrm{Fe}} + H_K^{\mathrm{Fe}}$$
$$H_0^{\mathrm{Fe}} = \sum \varepsilon_0^{\mathrm{Fe}} \hat{n}_{nm\sigma}^{\mathrm{d}},\ H_0^{\mathrm{Si}} = \sum \varepsilon_0^{\mathrm{Si}} \hat{n}_{nm\sigma}^{\mathrm{p}}.$$

The Kanamori's part of the Hamiltonian is

$$H_K^{\mathrm{Fe}} = \frac{U}{2}\sum \hat{n}_{nm\sigma}^{\mathrm{d}} \hat{n}_{nm\bar{\sigma}}^{\mathrm{d}} + \left(U' - \frac{1}{2}J\right)\sum \hat{n}_{nm}^{\mathrm{d}} \hat{n}_{nm'}^{\mathrm{d}}(1-\delta_{mm'}) - \frac{1}{2}J\sum \hat{\boldsymbol{s}}_{nm}^{\mathrm{d}} \hat{\boldsymbol{s}}_{nm'}^{\mathrm{d}}. \tag{2}$$

The Hamiltonian of the interatomic exchange and hopping parts is

$$H_{J'}^{\mathrm{Fe-Fe}} = -\frac{1}{2}J'\sum \hat{\boldsymbol{s}}_{nm}^{\mathrm{d}} \hat{\boldsymbol{s}}_{n'm'}^{\mathrm{d}};$$
$$H_{\mathrm{hop}} = \sum T_{n,n'}^{mm'} p_{nm\sigma}^{\dagger} p_{n'm'\sigma} + \sum t_{n,n'}^{mm'} d_{nm\sigma}^{\dagger} d_{n'm'\sigma} + \sum \left[(t')_{n,n'}^{mm'} d_{nm\sigma}^{\dagger} p_{n'm'\sigma} + \mathrm{H.c.}\right]; \tag{3}$$

where

$$\hat{n}_{nm\sigma}^{\mathrm{d}} \equiv d_{nm\sigma}^{\dagger} d_{nm\sigma};\quad \hat{n}_{nm}^{\mathrm{d}} = \hat{n}_{nm\uparrow}^{\mathrm{d}} + \hat{n}_{nm\downarrow}^{\mathrm{d}};\quad \hat{\boldsymbol{s}}_{nm}^{\mathrm{d}} \equiv \boldsymbol{s}_{\alpha\gamma} d_{nm\alpha}^{\dagger} d_{nm\gamma};$$
$$\hat{n}_{nm\sigma}^{\mathrm{p}} \equiv p_{nm\sigma}^{\dagger} p_{nm\sigma}. \tag{4}$$

Here $p^{\dagger}$ (p) are the creation (annihilation) operators of p-electrons of Si and $d^{\dagger}$ and d stand for d-electrons of Fe ions; n is the complex lattice index (site, basis); m labels the orbitals; the indices σ, α, γ are spin projections; $\boldsymbol{s}$ are Pauli matrices; U, $U' = U - 2J$ and J are the intra-atomic Kanamori parameters; J' is the parameter of the intersite exchange between the nearest Fe atoms. Finally, $T_{n,n'}^{mm'}$, $t_{n,n'}^{mm'}$ $(t')_{n,n'}^{mm'}$ are hopping integrals between Si–Si, Fe–Fe and Fe–Si atomic pairs, respectively.

The dependencies of hopping integrals on the wave vector k were obtained from the Slater and Koster atomic orbital scheme[18] in the two-center approximation using a basis set consisting of five 3d orbitals for each spin on each Fe atom and three 3p orbitals for each spin on each Si atom. Then, within the two-center approximation, the hopping integrals are expressed in terms of the Slater–Koster parameters $t_\sigma \equiv (\mathrm{dd}\sigma)$, $t_\pi \equiv (\mathrm{dd}\pi)$ and $t_\delta \equiv (\mathrm{dd}\delta)$ for Fe–Fe hopping and $t_\sigma \equiv (\mathrm{pd}\sigma)$, $t_\pi \equiv (\mathrm{pd}\pi)$ for Fe–Si and Si–Si hopping. In calculations of the model phase diagrams (maps) for magnetic moments we neglected the weak δ-bonds ($t_\delta = 0$) for Fe–Fe hopping and kept fixed the relations $t_\pi = t_\sigma/3$ for the nearest neighbors (NN) Fe–Si ($t_\sigma \equiv t_{\mathrm{Fe-Si}}$) and $t_\pi = t_\sigma/2$ for the next nearest neighbors (NNN) Fe–Fe ($t_\sigma \equiv t_{\mathrm{Fe-Fe}}$) and Si–Si ($t_\sigma \equiv t_{\mathrm{Si-Si}}$) and $t_\pi = t_\sigma/2$. We assume that hopping integrals depend on the distance R between the ions exponentially:

$$t(R) = t^{\max}\exp(-\gamma\Delta R), \tag{5}$$

where $t^{max} = t(R_{min})$ and $\Delta R = R - R_{min}$ (Å). We have found the parameters $\gamma_1 = 0.89$ Å^{-1} for t_{Fe-Fe}, $\gamma_2 = 0.93$ (Å^{-1}) for t_{Fe-Si}[10] and $\gamma_3 = 0.94$ Å^{-1} for t_{Si-Si}.

We should note that, although according to Harrison[19] this contribution should scale with the atom–atom distance, d, as d^{-2}, the concrete form of the scaling becomes non-essential for small distortions (3%), especially because the fit has been performed to the results of the *ab initio* calculations. For this reason we choose the exponential form for the scaling of the hopping matrix element as a more appropriate choice for the discussion of magnetism.

To determine the parameters of the model, we used the method of self-consistent mapping, described in detail in ref. 10 and 12 and in Appendix A (see the ESI†). Following[10,12] the model parameters can be found from minimization of the difference $Y = [\rho_{GGA}(k,\sigma) - (\rho_{model}(k,\sigma); U, U', J)]^2$ between the "genuine" electron density $[\rho_{GGA}(k,\sigma)]$ and the model one $(\rho_{model}(k,\sigma); U, U', J)$ with respect to interaction parameters U, U', J.[10,12] Since the Hartree–Fock equations have to be solved self-consistently for each set of model parameters, we simplified the problem further and, instead of minimization of function Y (*i.e.*, the differences of the model and VASP electron spin densities in each point of space), we've chosen to fit the number of d-electrons, the magnetic moments and partial d-densities of state (d-DOS) for Fe atoms (see eqn (5) in ref. 10). We perform several attempts during the fitting procedure: (1) as an initial guess for the fitting procedure we choose as the occupation numbers obtained within the *ab initio* approach as well as the ferromagnetic configuration of magnetic moments; (2) we start as with zero values of the Slater–Koster parameters as well as with arbitrary parameters. Then, we conduct fitting and choose the parameters which provide the best agreement. Note that all obtained sets give qualitatively the same results. During the fitting of the densities of state we primarily focus on the energy interval near the Fermi energy $[-3.0; 2.0]$ eV.

The model parameters for the undistorted α-$FeSi_2$ providing the best fit to the *ab initio* calculation were obtained in ref. 10: on-site parameters $U = 1$ eV, $J = 0.4$ eV, $\varepsilon_{Si} = 6$ eV, $\varepsilon_{Fe} = 0$ and the hopping integrals $t_{Fe-Fe} = -0.7$ eV, $t_{Fe-Si} = 1.0$ eV, $t_{Si-Si} = 1.75$ eV. On-site parameters during all model calculations were kept fixed. In the rest of the paper all hopping parameters are given in eV.

III. Results and discussion

A. The effect of lattice distortions on magnetism formation

The compound α-$FeSi_2$ has a tetragonal unit cell (space group $P4/mmm$) with the lattice parameters $a = b = 2.7$ Å and $c = 5.13$ Å. Its structure is shown in Fig. 1a. In the undistorted α-$FeSi_2$ the iron atoms are located at (0,0,0), optimized fractional coordinates of the Si atoms are (0.5,0.5,0,272) and (0.5,0,5,0.728). As seen from Fig. 1a there is a cavity between the Si atoms in the structure due to the large distance between Si atoms along the tetragonal c-axis ($R_{Si-Si} = 2.4$ Å). The calculated equilibrium distance between Fe–Si atoms $R_{Fe-Si} = 2.36$ Å. Our DFT-GGA calculations confirm that the ground state of α-$FeSi_2$ is non-magnetic metal.[20] The full densities of electron state (DOS) of α-$FeSi_2$ are shown in Fig. 2a. The peak in the DOS in the vicinity of the Fermi energy is mainly due to the e_g d-electrons (Fig. 2b, black line).

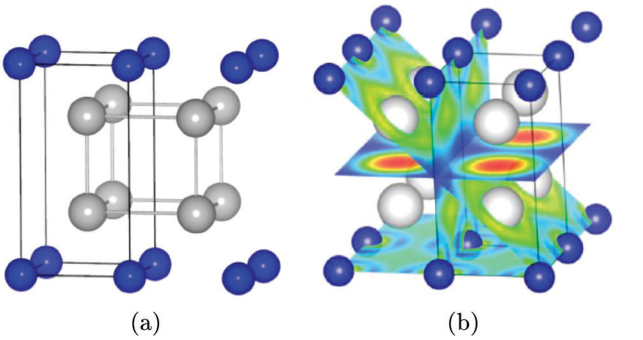

Fig. 1 (a) The crystal structure of α-$FeSi_2$; (b) the electron localization function (ELF) for α-$FeSi_2$. The degree of the electron localization on the color map spans from fully delocalized at the blue and green end, to the yellow and red for localized electrons. "Channels" of strongly delocalized electrons are located in the middle plane perpendicular to the c-axis. The blue balls stand for the Fe atoms, the grey ones are for the Si atoms.

It is interesting to note that according to the electron localization function[20] (Fig. 1b) the electron cloud forms elongated regions of strongly delocalized electrons between the planes of the silicon atoms. These regions look like channels. One may expect that (a) the effective single-electron wave function of these electrons is close to a simple plane wave $\sim\exp(i\boldsymbol{kr})$ along the c-axis and (b) these channels can be a source for an anisotropy of conductivity. For this reason we call them "conducting channels". However, the question of whether these particular states have their energies in the vicinity of the Fermi surface or not is, at the moment, still open. Furthermore, we are not aware of any experimental inspection of this question. These "channels" are elongated areas of delocalized electrons, shown in Fig. 1b in blue.

While α-$FeSi_2$ in the bulk form is non-magnetic, there are several experimental studies where ferromagnetism is found in thin films[7] and nanoparticles.[8,9] Recently[11] nano-sized grains of [001]-faceted α-$FeSi_2$ have been synthesized on a silicon substrate. Magnetic measurements indicated the existence of a small magnetic moment (MM), $\sim 0.2\ \mu_B$ per Fe atom. According to experimental data[11] the spacing between Fe layers along the tetragonal axis in the obtained nano-grains is changed compared to that in the bulk; it is larger between the layers which are close to the substrate surface and decreases further from the substrate and then again increases. This behavior is a manifestation of Friedel's oscillations of the density of electron gas near a surface or interface (see ref. 21 and 22). It is well-known fact that the positions of minima in electron density and, respectively, in energy, are very sensitive to the variation of the boundary conditions. In addition to this, stresses of $\sim 1.2\%$ arise in the plane perpendicular to the c axis, which are caused by mis-fitting with the silicon substrate. These stresses induce an increase of the distance R(Fe–Fe) between the iron atoms in this plane.

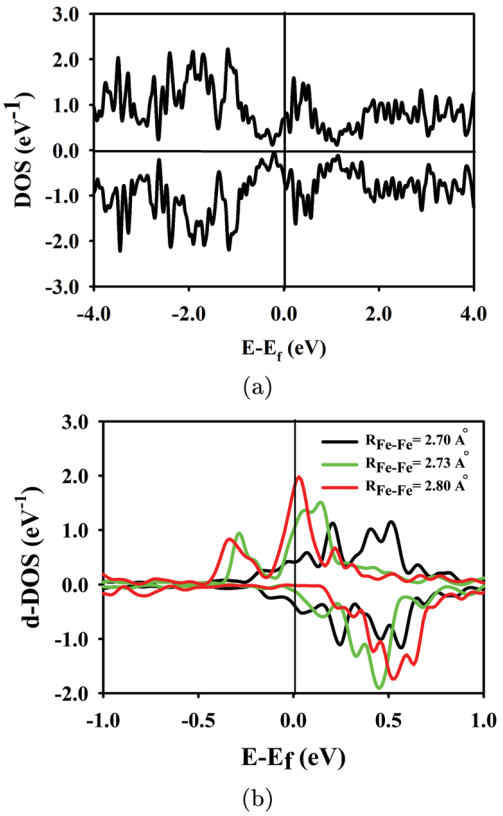

Fig. 2 (a) Full DOS for α-$FeSi_2$; (b) e_g-DOS of α-$FeSi_2$ (black line), supercell with R_{Fe-Fe} = 2.73 Å (green line), supercell with R_{Fe-Fe} = 2.8 Å (red line). Zero on the energy axis is the Fermi energy. The positive and negative values of DOS correspond to the spin-up and spin-down states, respectively.

In our earlier work[10] we have shown that ferromagnetism can be induced by external stresses as well as by insertion into the structure of additional atoms of iron or silicon. Contrary to this suggestion,[8,9] which explains the appearance of magnetism in nanoparticles of α-$FeSi_2$ by the formation of Fe clusters, the results of our theoretical analysis, together with experimental results,[11] indicate that the stresses alone may switch on the mechanisms of the MM formation in α-$FeSi_2$. The reaction of the magnetic subsystem to different types of distortions still remains unclear. The expectation we are going to inspect is that the MMs in α-$FeSi_2$ must be sensitive to changes in the distance between layers of iron and/or silicon.

These experiments[11] demonstrated that the magnetic properties of α-$FeSi_2$ do depend on the interlayer distance R_{IL}. It remains unclear, however, to what extent this factor is important for the formation of a magnetic moment in this compound. We performed *ab initio* calculations for the model supercell 1 × 1 × 4 with different R_{IL} (from 5.13 Å to 5.4 Å) between the Fe planes along the tetragonal axis. The stress arising from the substrate is modeled by a 1.2% increase of the distance between the in-plane iron atoms (R_{Fe-Fe} = 2.73 Å) compared to that in the bulk α-$FeSi_2$ (R_{Fe-Fe} = 2.70 Å). The optimization of the supercell with respect to the atomic coordinates results in a change of the interlayer distances between the Fe and Si planes (on average by about 3%) compared to those in the bulk. These changes induce MMs of about 0.2 μ_B on the Fe atoms in accordance with experimental data.

The partial contribution to the DOS from e_g-electrons of Fe for this model supercell is shown by the green (on-line) curve in Fig. 2b. The lattice distortion of the parent α-$FeSi_2$ shifts the e_g-electron peaks in the spin-up and spin-down DOS relative to each other and increases the spin polarization by about 70% in the model supercell. The latter is one of the most important characteristics for spintronic applications. An increase of the lattice parameter up to R_{Fe-Fe} = 2.8 Å leads to further amplification of these peaks in the DOS and to the strong increase of the spin polarization (Fig. 2b, red line).

Thus, the *ab intio* calculations indicate that an increase of merely the distance between in-plane Fe atoms results in the appearance of small magnetic moments. In order to obtain moments of at least $\simeq 0.3\ \mu_B$ per atom, the lattice parameter of α-$FeSi_2$ has to be increased by ∼5% (R_{Fe-Fe} = 2.8 Å), while an increase of the moment to $\sim 0.7\ \mu_B$ per atom requires an increase of the iron–iron distance up to ∼3 Å, *i.e.*, approximately, by 10%! Although distortions always arise when an α-$FeSi_2$ film is experimentally synthesized on an Si substrate, it never reaches such a large value. The experiment,[11] however, shows that the MM ∼ 0.2–0.3 μ_B per atom arises in nanoparticles of α-$FeSi_2$ at a smaller misfit strain, ∼1.2%. This fact implies that nsome other mechanisms of moment formation can possibly be switched on by or during synthesis of α-$FeSi_2$ films. The simplest ones are just other, different types of distortions. There are several types of bulk-α-$FeSi_2$-lattice distortions which may cause the appearance of magnetism in our model supercells. It can be either an increase of the distance between Fe atoms in the plane, or a change of the distance R_{Si-Si} between silicon atoms, or even the distance R_{Fe-Si} between iron and silicon atoms. Below we examine these possibilities in detail.

A convenient tool for this is the mapping of the results, obtained by the first-principle calculations, to the multiple-orbital model described in ref. 10 and 12 and briefly outlined in Section IIB. According to the results,[10] the main parameter which controls MM formation is the hopping integral t_{Fe-Fe} between the in-plane Fe atoms (Fig. 3). The blue point on Fig. 3 shows the values of hopping integrals (t_{Fe-Fe} = −0.7 eV, t_{Fe-Si} = 1.0 eV, t_{Si-Si} = 1.75 eV) which provide the best fit to the *ab initio* charge density for bulk α-$FeSi_2$.

The parameters for Fe–Si hopping t_{Fe-Si} and Si–Si hopping t_{Si-Si} seem intuitively to be non-relevant to MM formation. As will be seen below, this expectation is not supported by calculations. *Via* the self-consistent solution of the model equations for the population numbers of orbitals and the magnetization within the Hartree–Fock approximation, we obtained the MM map in the coordinates t_{Fe-Si} *vs.* t_{Si-Si} at the fixed value of t_{Fe-Fe} = −0.7 eV (Fig. 4a). The latter value corresponds to the equilibrium Fe–Fe distance R_{Fe-Fe} = 2.7 Å for bulk α-$FeSi_2$. Note that a decrease of the distance between silicon atoms, R_{Si-Si}, increases the distance between the Fe and Si atoms, and *vice versa* (Fig. 1a). As seen from the map in Fig. 4a, there is no magnetism at the equilibrium distance

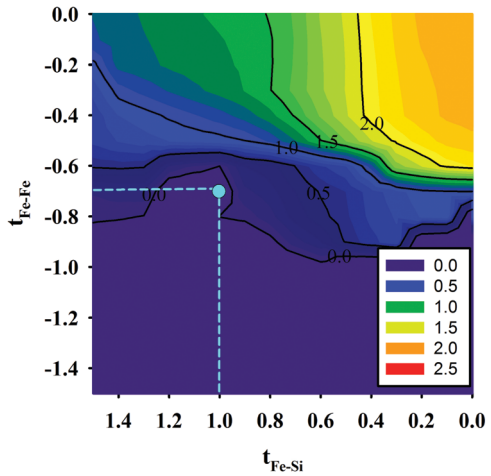

Fig. 3 The map of magnetic moments $M(t_{Fe-Fe},t_{Fe-Si})$ for α-$FeSi_2$ at the equilibrium lattice parameter. Dashed blue lines and the blue point show the values of hopping integrals which provide the best fit to the *ab initio* charge density. The values of hopping parameters are given in eV.

R_{Fe-Fe} = 2.7 Å in undistorted α-$FeSi_2$. However, a decrease of the hopping integral t_{Fe-Si} with a simultaneous increase of t_{Si-Si} leads to the arising of the magnetism at the same distance R_{Fe-Fe}. As seen from the upper left corner of the map Fig. 4a, a large MM ∼ 1–1.1 μ_B can be achieved by a decrease of the distance between Si atoms which causes a change of the hopping integral magnitudes. So, hopping integrals $t_{Si-Si} \approx 3.1$ and $t_{Fe-Si} \approx 0.5$ correspond to distances $R_{Si-Si} \approx 1.6$ Å and $R_{Fe-Si} \approx 2.6$ Å. And, *vice versa*, an increase of the Si–Si distance (a decrease of t_{Si-Si} and increase of t_{Fe-Si}) leads to a decrease of the MM to ∼0.1–0.3 μ_B.

Thus, the analysis of the model within the Hartree–Fock approximation shows that the ferromagnetic state in α-$FeSi_2$ may be induced by: (a) the increase of the distance between iron atoms (Fig. 3); and (b) the change of the distance between NN (nearest neighbors) silicon and iron atoms, and between silicon atoms (Fig. 4a). An application of both types of changes expands the area of existence of the ferromagnetic solutions. This is illustrated by Fig. 4b, which displays the map of MMs evaluated at $t_{Fe-Fe} = -0.65$ eV. This corresponds to R_{Fe-Fe} = 2.78 Å, according to eqn (5); *i.e.*, to the misfit strain ∼3%. At this distance the magnitudes of the MM, $M \sim 1.0\ \mu_B$, arise at smaller hoppings (Fig. 4b) $t_{Si-Si} \approx 2.7$ ($R_{Si-Si} \approx 1.8$ Å) and $t_{Fe-Si} \approx 0.65$ ($R_{Fe-Si} \approx 2.5$ Å).

In order to confirm the model findings we performed *ab initio* calculations of the moment dependence on the distances between silicon atoms in α-$FeSi_2$. Fig. 5 displays the comparison of the results of model and *ab initio* calculations for the dependence of the MM at iron atoms on the silicon–silicon distance R_{Si-Si} at equilibrium and the expanded R_{Fe-Fe} distances between in-plane iron atoms. Similar to the model result, a decrease of R_{Si-Si} causes a sharp increase of the MM. Note that a slight increase of R_{Si-Si} also may induce MM, but in this case the moment is small. An increase of the distance between iron atoms leads to the appearance of a large moment at the same distance R_{Si-Si}. Fig. 5 confirms that the results of the model and the *ab initio* calculations are in qualitative agreement with each other.

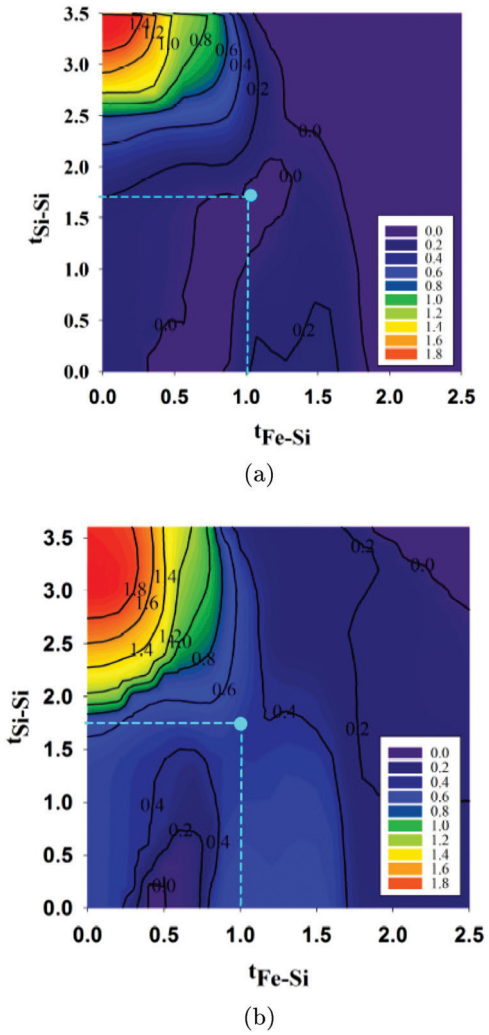

Fig. 4 The map $M(t_{Fe-Si},t_{Si-Si})$ of magnetic moments M for α-$FeSi_2$: (a) at equilibrium lattice parameter a = 2.7 Å; (b) at a = 2.8 Å. Dashed blue lines and the blue points show the values of hopping integrals which provide the best fit to the *ab initio* charge density. The values of hopping parameters are given in eV.

The analysis performed in this part can be summarized as follows. Both the model and *ab initio* calculations indicate that the ferromagnetism in α-$FeSi_2$ can be induced by different types of lattice distortions: not only by an increase of the in-plane distance between iron atoms, but also by a change of the distance between layers along the tetragonal axis. The latter alters iron–silicon and silicon–silicon interatomic distances (see Fig. 5). The decisive parameter for MM formation is the iron–iron distance in the plane perpendicular to the tetragonal axis c (Fig. 3 and 4). However, in order to obtain moments large enough for practical applications, the required misfit strain has to be made quite large, ∼10–15%. Such big magnitudes can hardly be achieved experimentally. At the experimentally feasible range of the misfit strain 1–3% the MM remains small. The other solution consists of a simultaneous decrease of the Si–Si distance (R_{Si-Si}) and an increase of the Fe–Si and Fe–Fe distances. Indeed, as seen

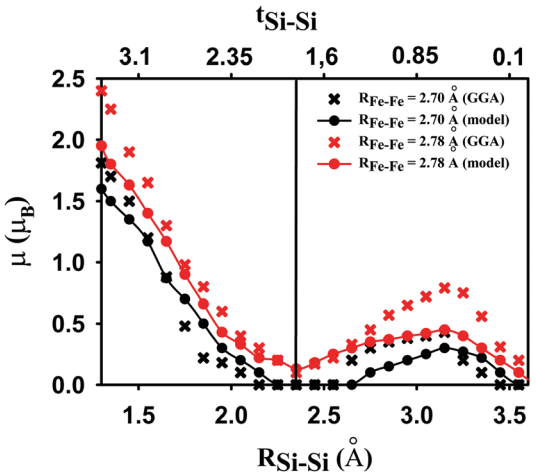

Fig. 5 The dependence of the MM in α-$FeSi_2$ on the distance R_{Si-Si} between silicon atoms (the hopping integrals in the model $t = t(R_{Si-Si})$). The results for R_{Fe-Fe} = 2.7 Å are displayed by the black color and for R_{Fe-Fe} = 2.78 Å by red. The crosses stand for GGA (in VASP), the points with a solid line are for the model within the HFA. The vertical line indicates the equilibrium distance R_{Si-Si} = 2.34 Å in α-$FeSi_2$. The values of hopping parameters are given in eV.

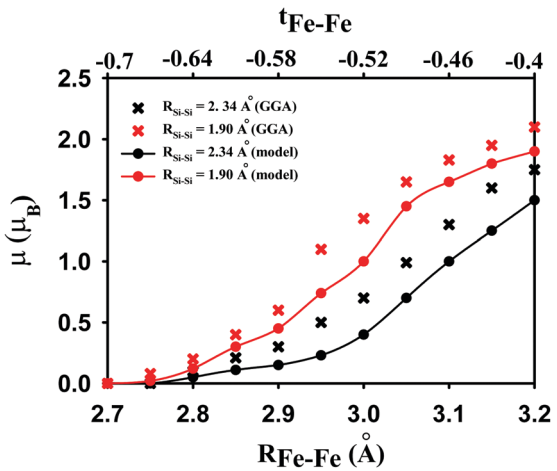

Fig. 6 The dependence of the MM in α-$FeSi_2$ on the distance R_{Fe-Fe} between iron atoms (the hopping integrals in the model $t = t(R_{Fe-Fe})$). The results for R_{Si-Si} = 2.34 Å are displayed by the black color and for R_{Si-Si} = 1.90 Å by red. The crosses stand for GGA (in VASP), the points with a solid line are for the model within the HFA.

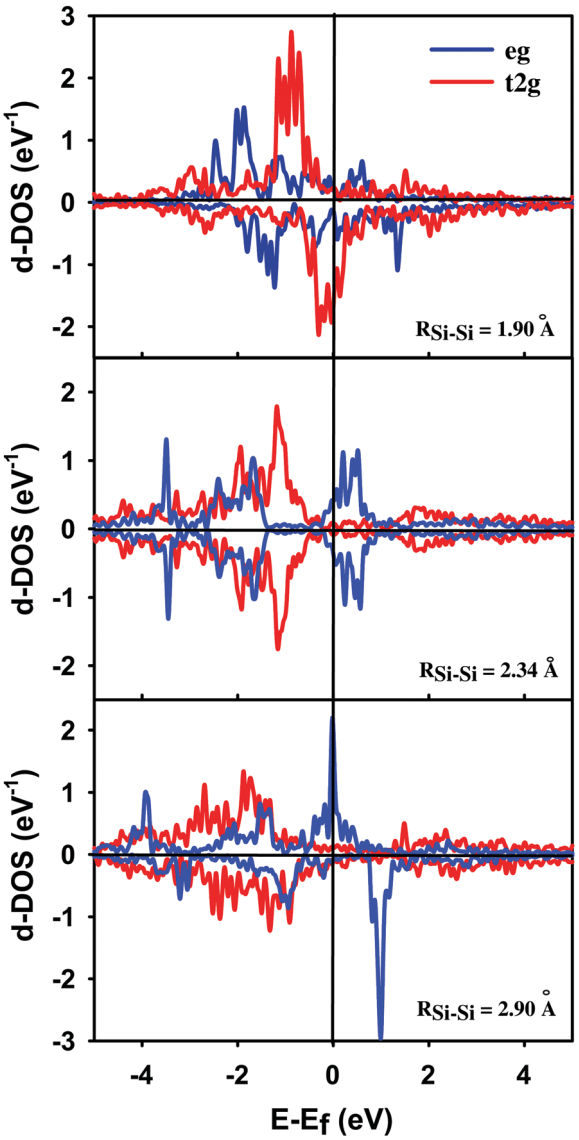

Fig. 7 Partial densities of d-states of α-$FeSi_2$ for different lattice distortions. From top to bottom: R_{Si-Si} = 1.90 Å, the equilibrium R_{Si-Si} = 2.34 Å, R_{Si-Si} = 2.90 Å. The t_{2g}-DOS is displayed by red (on-line) and the e_g ones by the blue color. Zero on the energy axis is the Fermi energy. The positive and negative values of DOS correspond to the spin-up and spin-down states, respectively.

from Fig. 6, where the dependence of the on-iron-MM on the distance R_{Fe-Fe} at R_{Si-Si} = 2.34 Å and R_{Si-Si} = 1.9 Å is displayed; the decrease of R_{Si-Si} gives rise to a larger MM at the same Fe–Fe distance.

Another way to understand why some of the lattice distortions favor the appearance of magnetism is to analyze the evolution of the partial density of d-electron states (d-DOS) with these distortions. As shown in Fig. 7 the decrease of the distance between silicons (R_{Si-Si}) shifts the peaks of the $t_{2g}^{\downarrow}$ states, which move towards the Fermi level. This, in turn, gives rise to spin polarization. However, an increase of R_{Si-Si} or the distance R_{Fe-Fe} between the iron atoms shifts not the t_{2g}-, but the e_g-peaks. In this case the $e_g^{\updownarrow}$-states appear near the Fermi level, providing a non-zero spin polarization.

The analysis given above highlights the main difficulty which is expected to arise in experiments upon inducing a magnetism in α-$FeSi_2$ with reasonably large MM *via* lattice distortions. Particularly, the MM $\simeq$ 1.0 μ_B should arise at $R_{Fe-Fe} \simeq 3$ Å, or $R_{Si-Si} \simeq 1.8$ Å ($R_{Fe-Si} \simeq 2.5$ Å). Such distances between atoms are hardly possible to implement in α-$FeSi_2$ films with any type of substrate. The distortions which arise when the α-$FeSi_2$ is grown on the silicon substrate are much smaller; in the experiments[11] on α-$FeSi_2$ nanoparticles the magnitudes of the distortions between in-plane iron atoms are about 1%, while for interlayer distances this is about 5%.

Such small distortions induce, correspondingly, a small MM. The question arises, would it be possible to overcome this difficulty with a "chemical pressure"?

B. The effect of intercalation on the magnetism formation

As was mentioned above, there is a cavity between Si atoms in the α-$FeSi_2$ structure (Fig. 1a). An intercalation of other atoms into this cavity will distort the lattice. Here we investigate if intercalated atoms can introduce a change of the distances R_{Fe-Fe} and R_{Si-Si} sufficient for the appearance of magnetism. In order to check this hypothesis we performed *ab initio* calculations of α-$FeSi_2$ with embedded atoms of different elements.

The two types of positions for embedding the guest atoms are shown at Fig. 8. The location of intercalated atom at Si–Si or Fe–Fe bonds are the most energetically favorable. To check the stability of the intercalated structures we have calculated the energies of structures with intercalated atoms displaced from their equilibrium positions (Fig. 8). The energy of any such structure is always higher than energy of a structure with intercalated atoms in equilibrium positions. Moreover, the optimization procedure results in the return of the displaced intercalated atom to a position in the center of the Si cage (for metal atoms) or in the Si–Si bond (for non-metal atoms).

The non-metal atoms are found to prefer the positions on the bonds between the silicon atoms (Fig. 8a), whereas the position inside the tetragonal cavity formed by the silicon atoms is more energetically favorable for metal atoms (Fig. 8b). It is possible that other structures will form during thin film growth at 50% or 100% concentrations of intercalated atoms. However, we did not check this since the problem of the crystal structure prediction of the "alloys" requires special consideration and separate work. In the present paper we restrict ourselves to the structures shown in Fig. 8.

The intercalated atoms create a negative chemical pressure which results in an increase of the distance between host atoms compared to pure α-$FeSi_2$. The results of calculations for a 100% concentration of embedded atoms are summarized in Table 1, where the parameters of the lattice cell, the values of the MMs at the iron atoms and the spin polarization in some of the considered structures are shown. In this case the symmetry of intercalated structures remains the same as for the pure α-$FeSi_2$ ($P4/mmm$).

The enthalpies of formation were calculated as

$$H_f = E(\alpha\text{-}FeSi_2 + X) - N_{Fe}E_{Fe}^{bulk} - N_{Si}E_{Si}^{bulk} - N_X E_X^{ref} \quad (6)$$

where reference energies E_X^{ref} were calculated for molecular N_2, H_2, O_2 and for bulk materials in other cases; N_{Fe}, N_{Si}, N_X = the number of Fe, Si and intercalated atoms, respectively. Unfortunately, GGA approximation often fails badly on molecular O_2, giving large errors with respect to experimental formation energies. Therefore we use the correction factor $C = -1.2$ eV per O_2 ($E_{O_2}^{ref} = E_{O_2}^{GGA} + C$) from ref. 23 for calculation of the reference energy $E_{O_2}^{ref}$ of the oxygen molecule. The calculated enthalpies for a 100% concentration of intercalated atoms are given in the last column of Table 1. All obtained enthalpies are negative and, therefore, all considered structures are stable.

As seen from Table 1, an intercalation does not always lead to the formation of a magnetic state. *E.g.*, the structures with intercalated nitrogen atoms are not magnetic (see Table 1). Nevertheless, the general tendency of an MM increase with the increase of lattice distortion, as studied in the previous section, is reproduced by direct calculation. Note that the appearance of MM on Fe atoms is primarily related to lattice distortions produced by the intercalants. So, in the case of intercalation by a lithium atom when the intercalant atom is removed while the distortions are preserved, the magnetic moment is only slightly decreased (M_{Fe} = 0.75 μ_B). The same is observed for intercalation by nonmetal atoms. So, in the case of intercalation by an oxygen atom in a distorted structure without an intercalant atom, MM decreases down to M_{Fe} = 0.32 μ_B; and *vice versa*, the embedding of intercalant atoms into an undistorted structure of α-$FeSi_2$ does not cause the appearance of MM on the Fe atoms. As expected, the magnitude of the MM at iron atoms

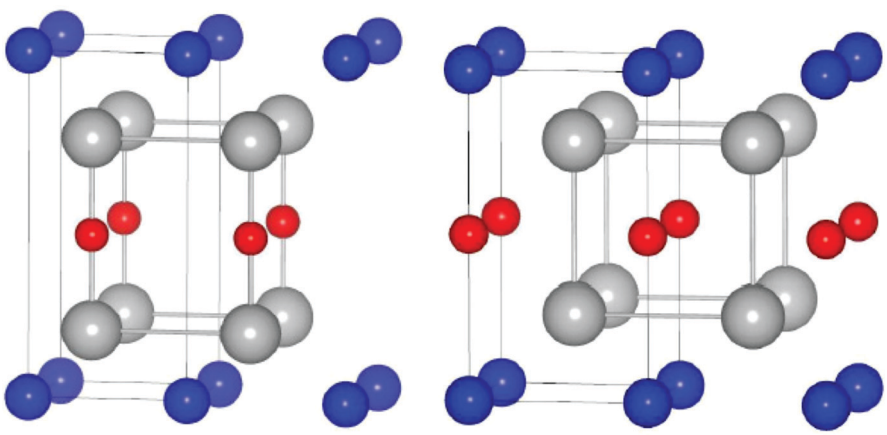

Fig. 8 Two possible positions for the embedding of an atom into the cavity between silicon atoms. (a) The positions occupied by non-metal atoms; (b) the positions occupied by metal atoms. Blue balls represent the Fe atoms, grey balls represent Si atoms, red balls represent intercalated atoms.

Table 1 The lattice parameters (a,c), magnetic moments on Fe atom (μ_{Fe}), the distance between Fe–Si (R_{Fe-Si}) and Si–X (X =intercalant) atoms (R_{Si-X}), spin polarization ($P = \frac{\rho^{\uparrow}(\varepsilon_F) - \rho^{\downarrow}(\varepsilon_F)}{\rho^{\uparrow}(\varepsilon_F) + \rho^{\downarrow}(\varepsilon_F)} \cdot 100\%$), anisotropy of the plasma frequency $\eta = \Omega_{xx}/\Omega_{zz}$ in the intercalated α-$FeSi_2$ and the formation enthalpies (H_f)

Atom X	Lattice parameters/Å		μ_{Fe} (μ_B)	R_{Fe-Si}/Å	R_{Si-X}/Å	P (%)	$\eta = \Omega_{xx}/\Omega_{zz}$	H_f/eV per N_X
Position 1 (Fig. 8a)								
H	2.72	6.28	0.20	2.37	1.76	0	0.52	−1.23
O	2.76	5.91	0.45	2.36	1.63	61	1.767	−0.92
P	2.71	7.27	0.47	2.28	2.35	75	1.63	−0.15
As	2.76	7.58	0.53	2.36	2.46	38	1.737	−0.11
Sb	2.89	7.80	0.90	2.40	2.64	38	2.12	−0.04
N	2.74	6.05	0.00	2.39	1.63	0	1.96	−1.06
Position 2 (Fig. 8b)								
Li	2.93	5.34	0.90	2.43	2.50	11	0.84	−0.09
Na	2.90	6.80	0.65	2.41	2.94	71	1.19	−0.03
K	2.87	8.07	0.14	2.44	3.36	68	2.68	−0.02
Ca	3.00	6.85	1.00	2.46	3.04	11	1.03	−0.33
Sr	3.09	7.02	1.05	2.50	3.16	11	1.09	−0.21
Cu	2.95	5.38	0.90	2.24	2.52	24	1.06	−0.12
α-$FeSi_2$	2.70	5.13	0.00	2.36	—	0	0.87	—

grows with increasing Fe–Fe distance, but an increase of only R_{Fe-Fe} does not provide the magnitudes of MM listed in Table 1. For example, an increase of in-plane distance R_{Fe-Fe} up to 2.95 Å in pure α-$FeSi_2$ leads to an MM at the Fe atom of $M_{Fe} \simeq 0.5\ \mu_B$ only (Fig. 6), whereas intercalation by some atoms increases MM by 1.5–2 times at the same R_{Fe-Fe}. The latter occurs due to additional structure distortions and corresponding restructuring of the DOS due to intercalated atoms.

These calculations show that the distortions caused by intercalation change the t_{2g}-DOS only slightly; the main changes occur in the e_g-DOS. Similar to pure α-$FeSi_2$ it is namely the e_g-DOS that forms the peaks in the vicinity of the Fermi level. This is illustrated in Fig. 9 for several intercalants; similar to pure α-$FeSi_2$ the increase of the distances R_{Fe-Fe} and R_{Si-Si} causes shifts of the $e_g^{\uparrow}$- and $e_g^{\downarrow}$-peaks. In the case of non-metallic intercalants (P, As, Sb) this shift grows with an increase of the distances R_{Fe-Fe} and R_{Si-X} (Fig. 9a). For the metallic intercalants Li, Na, K the tendency is opposite (Fig. 9b).

As seen from Fig. 9 and Table 1, intercalation of P and Na is expected to provide high spin polarization due to the crossing of the Fermi energy by the $d^{\uparrow}$-peaks of DOS. The quite strong spin polarization (7th column in Table 1) may occur not only in the cases of intercalation by the above-mentioned P and Na, but also by O and K. A small increase of the in-plane lattice parameter, which arises when the α-$FeSi_2$ is intercalated by H, As, O or P, allows for the use of the silicon substrate. The intercalation by Li, Na, K and Sb atoms results in a 7% increase of the in-plane lattice parameter compared to pure α-$FeSi_2$, but the compressive strain from the substrate can decrease this distortion. This, however, does not prevent MM completely, but decreases it by 30–40%. Therefore, one can expect that the choice of a substrate with a larger lattice parameter than that of silicon (*e.g.*, Ge) would allow a decrease of this misfit strain and increase the magnitude of MM.

Since it is hardly possible to achieve 100% concentration of intercalated atoms during experiment, we estimate the value of MM arising at the Fe atoms for lower concentrations of intercalated atoms; namely for 25% and 50% concentrations of intercalated atoms. In order to consider a possible ordering of intercalated atoms with these concentrations we constructed a 2 × 2 × 2 supercell of α-$FeSi_2$. Further calculations depend on the way that the sample is made. Annealing of a sample may switch on the thermodynamic equilibration processes, possibly ion migration, *etc.* This may exclude the contribution of less energetically favorable configurations. An estimation of the barriers for the migration of ions and the contribution of phonons is needed for a quantitative description of these processes. This requires special consideration. In the case when a sample is made by quenching, the situation is simpler: due to fast cooling of the sample the energy hierarchy of different possible configurations is much less important and their contribution to an averaged physical quantity $\langle A \rangle$ may be calculated either with the help of simple statistical weights, or by means of some kind of realization of the coherent potential approximation. The latter, however, also involves additional assumptions about the distribution function and the way that the effective medium is introduced (see, *e.g.*, ref. 24 and 25), but has the advantage that it does not require supercell calculations and can be used for an arbitrary (but not too small) concentration. Here we consider the first case.

A configurationally disordered structure may contain several locally different arrangements of intercalated atoms, each at their fixed concentration. Let us consider the possible arrangements and calculate their weights. Let us denote the statistical weights of the configurations i as $w_x^{(n)}(i)$, where x is the concentration of intercalated atoms, and n_x^i is number of equivalent configurations of the type i, and $A_x^n(i)$ is value of the physical quantity in the configurations i. Then the total number of configurations is $N_c(x) = \sum_i n_x^i w_x^{(n)}(i)$ and

$$\langle A \rangle = \frac{1}{N_c(x)} \sum_i A_x^{n_i}(i) n_x^i w_x^{(n)}(i). \quad (7)$$

For the 25% concentration of intercalating atoms we have $N_c(0.25) = \binom{8}{2} = 28$ arrangements. Five of them are different (see Appendix B in the ESI†). Considering all possible configurations we find that, for $x = 0.25$, the statistical weight $w_{0.25}^{(3)} = 4$ for three of them, and $w_{0.25}^{(2)} = 8$ for two of them. For a 50% concentration of intercalated atoms there are $N_c(0.5) = \binom{8}{4} = 70$ possible ways to distribute atoms. Nine of them are different (see Appendix B in the ESI†): for three configurations $w_{0.5}^{(3)} = 2$, for two it is $w_{0.5}^{(2)} = 4$, $w_{0.5}^{(2)} = 8$, $w_{0.5}^{(1)} = 16$, and $w_{0.5}^{(1)} = 24$ ($\sum_i n_{0.5}^i w_{0.5}^{(n)} = 70$).

We find that the prospective candidates are Li metal and the O non-metal intercalants. As seen from Table 1, the intercalation with these atoms results in relatively large MMs for comparatively small lattice distortions. We performed a full

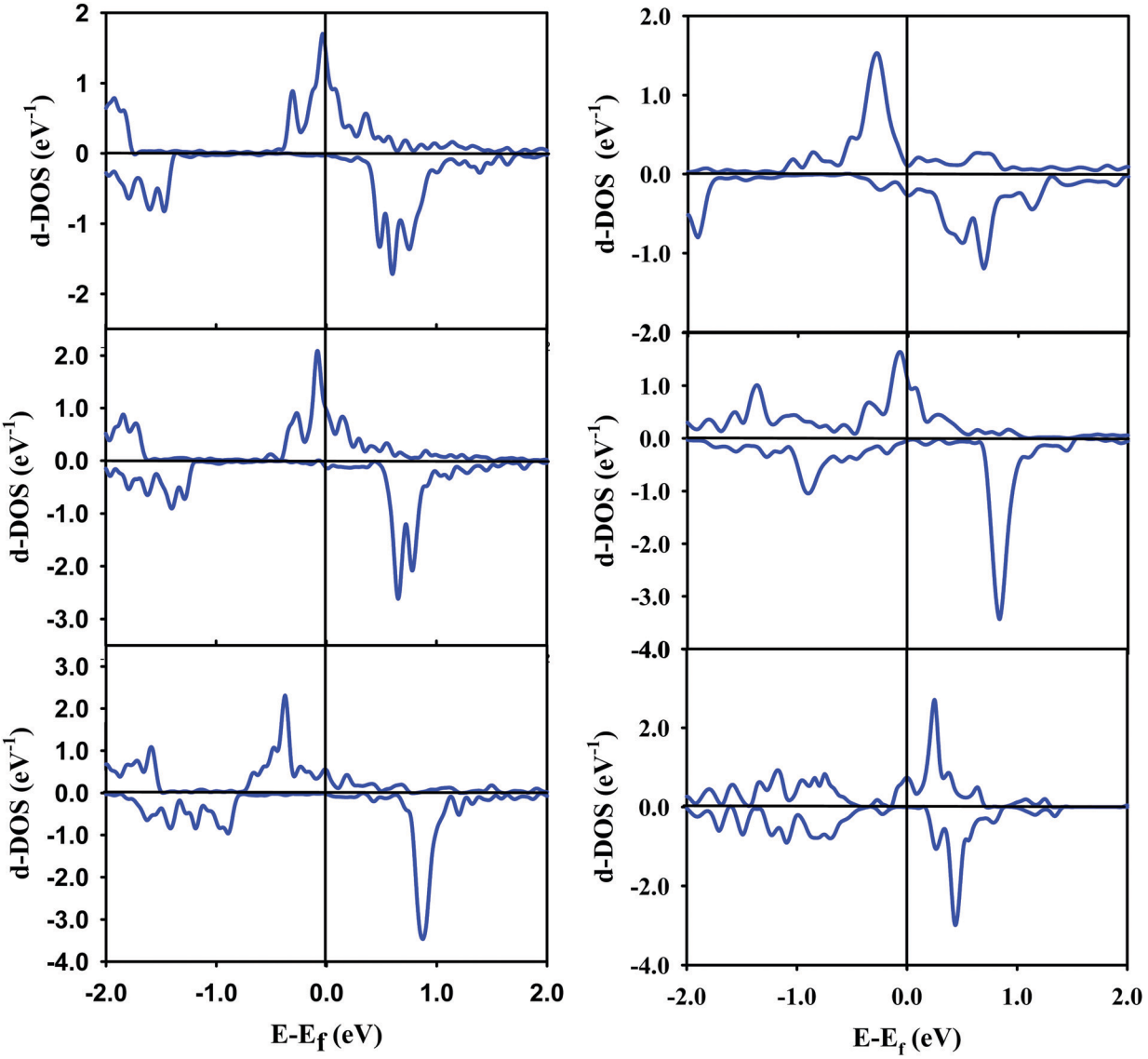

Fig. 9 (a) e_g-DOS for α-$FeSi_2$ intercalated by the non-metal atoms which occupy the first positions in Fig. 8; from top to bottom: P, As, Sb (b) e_g-DOS for α-$FeSi_2$ intercalated by the metal atoms (second position in Fig. 8); from top to bottom: Li, Na, K. Zero on the energy axis is the Fermi energy. The positive and negative values of DOS correspond to the spin-up and spin-down states, respectively.

optimization for all ordered structures. In Table 2 we give the difference $\Delta E = E_{max} - E_{min}$ between the maximal and minimal energies of the structures for each of these cases. The total energy values of different ordered structures are within 0.5 eV range per unit cell of α-$FeSi_2$. The average lattice parameters $\langle a \rangle$, $\langle c \rangle$ (Å), Fe MMs $\langle \mu \rangle$ (μ_B) and spin polarization $\langle P \rangle$ (%), calculated according to eqn (7) are given in Table 2. In the last row of Table 2 we give the averaged enthalpy of formation $\langle H_f \rangle$ (eqn (6)). Note that the enthalpy of formation of different ordered structures are within a few hundredths of eV per N_X.

Although at a 25% concentration of lithium atoms the lattice parameters have only little change as compared with α-$FeSi_2$ (Table 2), the average MM on Fe atoms is equal to 0.31 μ_B; an increase of concentration up to 50% results in the increase of

Table 2 The energy difference (ΔE) between maximal and minimal energies of ordered supercells of intercalated α-$FeSi_2$, average magnetic moments ($\langle \mu \rangle$), spin polarization ($\langle P \rangle$), lattice parameters ($\langle a \rangle$, $\langle c \rangle$) and formation enthalpies ($\langle H_f \rangle$) in ordered intercalated α-$FeSi_2$ for 25% and 50% concentrations of intercalated atoms of oxygen and lithium

	O		Li	
	25%	50%	25%	50%
ΔE (eV)	0.23	0.5	0.05	0.42
$\langle \mu \rangle$ (μ_B)	0.14	0.28	0.31	0.67
$\langle P \rangle$ (%)	61	63	57	35
$\langle a \rangle$ (Å)	2.72	2.74	2.77	2.82
$\langle c \rangle$ (Å)	5.43	5.66	5.14	5.19
$\langle H_f \rangle$ (eV per N_X)	−1.21	−0.98	−0.47	−0.20

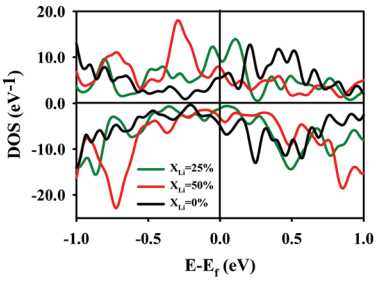

Fig. 10 Full DOS of Li-intercalated α-$FeSi_2$ for 0% (black line), 25% (green line) and 50% (red line) concentrations of intercalated atoms. Zero on the energy axis is the Fermi energy. The positive and negative values of DOS correspond to the spin-up and spin-down states, respectively.

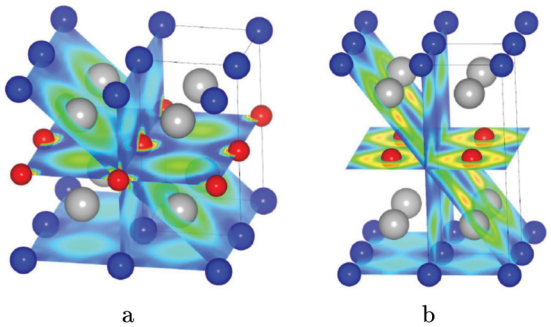

Fig. 11 The electron localization function (ELF) for (a) Li-intercalated α-$FeSi_2$; (b) P-intercalated α-$FeSi_2$. The degree of electron localization on the color map spans from fully delocalized at the blue and green end, to yellow and red for the localized electrons. Blue balls represent the Fe atoms, grey balls stand for Si atoms, red balls represent intercalated atoms.

MM up to 0.67 μ_B. Note that at the equilibrium lattice parameters of pure α-$FeSi_2$ without structure optimization by the atom coordinates, the MM on Fe atoms does not arise even at a 100% concentration of Li atom. This proves that the emergence of the magnetism in intercalated α-$FeSi_2$ is primarily associated with lattice distortions.

Note that in order to obtain a sample with a large spin polarization, the optimal concentration of Li intercalate has to be found. Indeed, since a move along the Li concentration from $x_{Li} = 0$ towards $x_{Li} = 1$ induces magnetism, the corresponding e_g – peak in the DOS moves from the region above the Fermi level E_f at $x_{Li} = 0$ to the region below it at $x_{Li} = 1$, while the $e_g^{\downarrow}$ – peak remains above E_f. In a certain concentration range the e_g – peak passes through E_f (see Fig. 10). In our case such a concentration is in the vicinity of $x_{Li} = 0.25$. The latter provides a large spin polarization. This conclusion is obtained for fully optimized structures.

When we intercalate α-$FeSi_2$ by non-metal oxygen atoms the value of the magnetic moment decreases with the decrease of oxygen concentration. However the spin polarization practically does not change with concentration. Fig. 9 shows that the positions of the d-electron peaks in DOS are much more sensitive to intercalation by heavier atoms (such as antimony), than by atoms of a metal. The intercalation by light oxygen or phosphorus atoms shifts the same d-electron peak much less with increase of concentration; at 100% concentration the peak is shifted by 0.25 eV, reaching the Fermi level.

Since there are preferable positions for the metal and non-metal intercalants, one may expect that the intercalation may cause an anisotropy of the compound properties. A standard way to estimate this effect would be to inspect the tensor of static electroconductivity σ_0, which in the VASP package is calculated by means of the Drude formula $\sigma_{\alpha\beta} = \tau\Omega_{\alpha\beta}^2/(4\pi)$. Here $\Omega_{\alpha\beta}$ is the plasma frequency and τ is the relaxation time. However, τ is the parameter which depends on many factors (like, *e.g.*, the method of preparation of the sample) and may differ for different samples even with the same concentration of intercalants, not to mention compounds with different intercalants. For this reason we prefer to estimate the degree of anisotropy of a compound just from the ratio $\eta = \Omega_{xx}/\Omega_{zz}$ (note that $\Omega_{xx} = \Omega_{yy}$). The results of these calculations are shown in Table 1, in the 8th column.

A question arises if the different preferable positions for the metal and non-metal atoms in lattice of α-$FeSi_2$ can be associated with the anisotropy? We inspected the maps of electronic localization function (ELF) at the intercalation by Li and P atoms (Fig. 11). For the non-metal atoms, which prefer to locate on the Si–Si bond, the "conducting channels" are shifted from the middle plane in the *c*-axis direction. The metal intercalated atoms prefer the position on the bond between out-of-plane Fe–Fe atoms. This leads to an overlap of the "conducting channels". The latter causes a more uniform distribution of the delocalized electrons by the volume of crystal (Fig. 11). Although this difference seems to exist for all metal and non-metal intercalated compounds, its contribution to anisotropy is not monotonic and it is difficult to formulate a general rule.

IV. Conclusion

The fact that a large, if not the decisive, role in the mechanism of magnetic structure formation in different compounds is played by the local environment of the magnetic species is well known from the physics of surface and interfaces. In earlier works,[10,12] in the framework suggested by our approach (hybrid self-consistent mapping (HSCMA)) we have shown that distortions of the crystal lattice as well as the types of atoms in the local environment have a significant impact on magnetic moment formation. According to the latest experimental data, α-$FeSi_2$ is predisposed to the appearance of its ferromagnetism. In ref. 10 we studied the possible reasons for this. As follows from the analysis of the map of the magnetic moment dependency on the hopping integrals, a crucial role in the appearance of ferromagnetism is played by the distortion of the crystal lattice in the Fe plane. A distinctive feature of all the calculated maps is the presence of sharp boundaries between regions with magnetic states and those that are non-magnetic. Therefore, the system is in the vicinity of magnetic instability and it is reasonable to assume that some other type of crystal-lattice distortions could cause the formation of a magnetic state in α-$FeSi_2$.

In the present work we consider the conditions which can lead to the appearance of magnetic state in α-$FeSi_2$. As follows from our model analysis, the magnetic state can arise not only when the distance between in-plane Fe–Fe atoms is changed, but also, for example, when the distance between out-of-plane Si–Si atoms is changed. Unfortunately, a pronounced magnetic moment can arise only during quite large distortions of the crystal lattice, even if a complex set of distortions is applied. We suggest that intercalation of α-$FeSi_2$ could be a way to solve this problem.

We used for this analysis an averaging procedure different from the one used in the well-known coherent potential approximation (CPA). Our method has the advantage that it takes into account the fact that the energies of different configurations at the same fixed concentration of dopants are different. The obvious disadvantage is that, contrary to the CPA method, it cannot be used at an arbitrary concentration. However, our method takes into account the short-range correlations at certain fixed concentrations, while the CPA method does not. Therefore, one can expect that a comparison of the results generated by the CPA and by our method at fixed concentrations can be used for estimation of the strength of the short-range correlations and a degree of their importance for the problem in question.

Our calculations indeed confirm that the intercalation of α-$FeSi_2$ results in the appearance of a significant magnetic moment on Fe atoms (0.5–1 μ_B) at relatively small lattice distortions (Table 1). It is apparent that it is hardly possible to reproduce the complex set of lattice distortions caused by the intercalated atoms only in the vicinity of interface by selecting different substrates for the film or nanoparticle fabrication; the intercalation has to be done for bulk α-$FeSi_2$.

In fact, for spintronics devices a large spin polarization is needed, not a large magnetic moment. We expect that (60–80%) spin polarization in α-$FeSi_2$ can be achieved *via* intercalation with certain elements, such as Li, P, Na, O. This can cause the required reconstruction of the electronic structure making, therefore, the intercalated α-$FeSi_2$ a promising candidate for application in spintronics. Note that although it is hardly possible to achieve 100% concentration of intercalated atoms in practice, the spin polarization remains large even at smaller concentrations. The advantage of maintaining a magnetic state at a smaller concentration of intercalated atoms is that smaller distortions of the lattice would facilitate the experimental fabrication of films on the silicon substrate, which is extremely important for modern silicate technology.

Conflicts of interest

There are no conflicts to declare.

Acknowledgements

The reported study was funded by the Russian Foundation for Basic Research, Government of Krasnoyarsk Territory, Krasnoyarsk Regional Fund of Science to the research projects No 17-42-240212: ''Quantum-mechanical simulation of the physical properties of correlated electron materials to improve their functional characteristics'' and No 18-42-243019: ''First-principles studies of the polarization, magnetic, electronic, and magnetoelectric properties of functional compounds with a spinel structure containing 3d and 4f ions''.

References

1 A. Wolf, D. D. Awschalom, R. A. Buhrman, J. M. Daughton, S. von Molnar, M. L. Roukes, A. Y. Chtchelkanova and D. M. Treger, Spintronics: a spin-based electronics vision for the future, *Science*, 2001, **294**, 1488–1495.

2 N. Jedrecy, A. Waldhauer, M. Sauvage-Simkin, R. Pinchaux and Y. Zheng, Structural characterization of epitaxial α-derived $FeSi_2$ on Si (111), *Phys. Rev. B: Condens. Matter Mater. Phys.*, 1994, **49**, 4725–4730.

3 M. Seibt, R. Khalil, V. Kveder and W. Schröter, Electronic states at dislocations and metal silicide precipitates in crystalline silicon and their role in solar cell materials, *Appl. Phys. A: Mater. Sci. Process.*, 2009, **96**, 235–253.

4 K. Yamaguchi and K. Mizushima, Luminescent $FeSi_2$ crystal structures induced by heteroepitaxial stress on Si(111), *Phys. Rev. Lett.*, 2001, **86**, 6006–6009.

5 Y. Makita, Y. Nakayama, Y. Fukuzawa, S. N. Wang, N. Otogawa, Y. Suzuki, Z. X. Liu, M. Osamura, T. Ootsuka, T. Mise and H. Tanoue, Important research targets to be explored for β-$FeSi_2$ device making, *Thin Solid Films*, 2004, **461**, 202–208.

6 J. Yuan, H. Shen and L. Lu, Influence of surface recombination and interface states on the performance of β-$FeSi_2$/c-Si heterojunction solar cells, *Phys. B*, 2011, **406**, 1733–1737.

7 G. Cao, D. J. Singh, X.-G. Zhang, G. Samolyuk, L. Qiao, C. Parish, K. Jin, Y. Zhang, H. Guo, S. Tang, W. Wang, J. Yi, C. Cantoni, W. Siemons, E. Andrew Payzant, M. Biegalski, T. Z. Ward, D. Mandrus, G. M. Stocks and Z. Gai, Ferromagnetism and nonmetallic transport of thin-film α-$FeSi_2$: A stabilized metastable material, *Phys. Rev. Lett.*, 2015, **114**, 147202.

8 J. K. Tripathi, M. Garbrecht, W. D. Kaplan, G. Markovich and I. Goldfarb, The effect of Fe-coverage on the structure, morphology and magnetic properties of α-$FeSi_2$ nanoislands, *Nanotechnology*, 2012, **23**, 495603.

9 J. K. Tripathi, G. Markovich and I. Goldfarb, Self-ordered magnetic α-$FeSi_2$ nano-stripes on Si(111), *Appl. Phys. Lett.*, 2013, **102**, 251604.

10 V. S. Zhandun, N. G. Zamkova, S. G. Ovchinnikov and I. S. Sandalov, Self-consistent mapping: effect of local environment on formation of magnetic moment in α-$FeSi_2$, *Phys. Rev. B*, 2017, **95**, 054429.

11 I. A. Tarasov, M. V. Rautskii, A. A. Dubrovsky, I. A. Yakovlev, L. A. Solovyov, T. E. Smolyarova, S. I. Popkov, M. N. Volochaev, S. N. Varnakov and S. G. Ovchinnikov, *ACS Appl. Mater. Interfaces*, to be published.

12 N. G. Zamkova, V. S. Zhandun, S. G. Ovchinnikov and I. S. Sandalov, Effect of local environment on moment formation in iron silicides, *J. Alloys Compd.*, 2017, **695**, 1213–1222.
13 G. Kresse and J. Furthmuller, Efficiency of *ab initio* total energy calculations for metals and semiconductors using a plane-wave basis set, *Comput. Mater. Sci.*, 1996, **6**, 15–50; G. Kresse and J. Furthmuller, Efficient iterative schemes for *ab initio* total-energy calculations using a plane-wave basis set, *Phys. Rev. B: Condens. Matter Mater. Phys.*, 1996, **54**, 11169–11186.
14 P. E. Blochl, Projector augmented-wave method, *Phys. Rev. B: Condens. Matter Mater. Phys.*, 1994, **50**, 17953–17979; G. Kresse and D. Joubert, From ultrasoft pseudopotentials to the projector augmented-wave method, *Phys. Rev. B: Condens. Matter Mater. Phys.*, 1999, **59**, 1758–1775.
15 J. P. Perdew, K. Burke and M. Ernzerhof, Generalized gradient approximation made simple, *Phys. Rev. Lett.*, 1996, **77**, 3865–3868; J. P. Perdew, K. Burke and M. Ernzerhof, Errata: Generalized gradient approximation made simple, *Phys. Rev. Lett.*, 1997, **78**, 1396.
16 H. J. Monkhorst and J. D. Pack, Special points for Brillouin-zone integrations, *Phys. Rev. B: Solid State*, 1976, **13**, 5188–5192.
17 J. Kanamori, Electron correlation and ferromagnetism of transition metals, *Prog. Theor. Phys.*, 1963, **30**, 275–289.
18 J. C. Slater and G. F. Koster, Simplified LCAO method for the periodic potential problem, *Phys. Rev.*, 1954, **94**, 1498–1524.
19 W. A. Harrison, *Electronic Structure and the Properties of Solids*, Freeman, San Francisco, 1980.
20 C. Kloc, E. Arushanov, M. Wendl, H. Hohl, U. Malang and E. Bucher, Preparation and properties of FeSi, α-$FeSi_2$ and β-$FeSi_2$ single crystals, *J. Alloys Compd.*, 1995, **219**, 93–96.
21 N. D. Lang and W. Kohn, Theory of metal surfaces: Charge density and surface energy, *Phys. Rev. B: Solid State*, 1970, **1**, 4555–4568.
22 J.-H. Cho, Ismail, Z. Zhang and E. W. Plummer, Oscillatory lattice relaxation at metal surfaces, *Phys. Rev. B: Condens. Matter Mater. Phys.*, 1999, **59**, 1677–1680.
23 S. Grindy, B. Meredig, S. Kirklin, J. Saal and C. Wolverton, *Phys. Rev. B: Condens. Matter Mater. Phys.*, 2013, **87**, 075150.
24 J. A. Blackman, D. M. Esterling and N. F. Berg, Generalized locator-coherent-potential approach to binary alloys, *Phys. Rev. B: Solid State*, 1971, **4**, 2412–2428.
25 W. Jones and N. H. March, *Theoretical Solid State Physics*, 1986, Dover Publications, Inc., New York, vol. 2, p. 1078.

